Equilibrium-range constant in wind-generated wave spectra

Donald T. Resio and Charles E. Long

Coastal and Hydraulics Laboratory, U.S. Army Engineer Research and Development Center, Vicksburg, Mississippi, USA

C. Linwood Vincent

Coastal Dynamics Program, Office of Naval Research, Arlington, Virginia, USA

Received 17 January 2003; revised 21 August 2003; accepted 6 October 2003; published 22 January 2004.

[1] The equilibrium range in wind-driven wave spectra is characterized to have an f^{-4} form in deep water ($k^{-5/2}$ shallow-water form). Absolute energy levels for six physically diverse sites are shown to be well fit by an expression involving the wind speed measured at a fraction of a wavelength above the sea surface in combination with the phase speed of the spectral peak. Observed energy levels suggest that nonlinear wave-wave interactions are capable of maintaining the observed energy-flux balance in the equilibrium range. *INDEX TERMS:* 4560 Oceanography: Physical: Surface waves and tides (1255); 4546 Oceanography: Physical: Nearshore processes; *KEYWORDS:* waves, ocean waves, wave spectra, nonlinear waves, air-sea interactions, equilibrium range

Citation: Resio, D. T., C. E. Long, and C. L. Vincent (2004), Equilibrium-range constant in wind-generated wave spectra, *J. Geophys. Res.*, *109*, C01018, doi:10.1029/2003JC001788.

1. Introduction

[2] The equilibrium range in wind wave spectra has long been a rich research topic for scientists, engineers and mathematicians. Though a strong tendency for wave spectra to exhibit an equilibrium form has long been known [*Phillips*, 1958; *Kitaigorodskii*, 1962; *Zakharov and Filonenko*, 1966], the exact cause of such a dynamic balance in this portion of the wave spectrum is still being debated. Many theoretical aspects of air-sea interaction and wind wave spectra, as well as practical considerations related to wave modeling, can be related to the characteristics of this balance. *Resio et al.* [2001] provide an historical perspective of the development of equilibrium range concepts for wind-generated wave spectra. Readers are referred to that paper for greater detail and only a brief synopsis of that introduction is repeated here.

[3] Initial equilibrium range concepts for waves in deep water were based solely on dimensional arguments and led to a spectral form of the type [*Phillips*, 1958]

$$E(f) \sim \alpha_5 g^2 (2\pi)^{-4} f^{-5}, \tag{1}$$

where $E(f)$ is spectral energy density in a frequency domain, α_5 is a dimensionless equilibrium range coefficient, g is gravitational acceleration and f is cyclic frequency. Within this theoretical framework, the coefficient α_5 in equation (1) was expected to be a universal constant since it was envisioned that wave breaking controlled energy levels in this part of the spectrum. If true, wind inputs, which become significant on a scale of tens or hundreds of wavelengths, would be negligible compared to breaking, which occurs over a scale of order one wavelength.

[4] Subsequent studies by *Mitsuyasu* [1968] and *Hasselmann et al.* [1973] provided clear evidence that α_5 was not a universal constant, but varied substantially as a function of certain dimensionless wave parameters that were all based on wind speed. At about the same time, the pioneering theoretical work of *Zakharov and Filonenko* [1966] and empirical results of *Toba* [1973] were providing evidence that a more appropriate form for the equilibrium range was

$$E(f) \sim \alpha_4 u g (2\pi)^{-3} f^{-4}, \tag{2}$$

where α_4 is a dimensionless equilibrium range coefficient appropriate for this class of spectra, and u is a scaling parameter with units of velocity. Many papers have now been written on both types of equilibrium range formulations, and it is generally conceded that the form of equation (2) is in better agreement with existing observations than that of equation (1).

[5] *Resio et al.* [2001] showed that the equilibrium range for finite depth wave spectra could be expressed in the wave number-equivalent form of equation (2) as

$$F(k) = \frac{\alpha_4}{2} u g^{-1/2} k^{-5/2}, \tag{3}$$

where $F(k)$ is spectral energy density in a wave number domain, and k is wave number (modulus), which is here related to f by the standard linear dispersion relation

$$(2\pi f)^2 = gk \tanh(kh), \tag{4}$$

where h is water depth. They showed that wave spectra written in this wave number basis continued to exhibit strong equilibrium range tendencies well into the finite depth range of frequencies. Using numerical simulations, they also showed that this form was consistent with the theoretical formulation of *Zakharov and Filonenko* [1966], even for cases of spectra with nonisotropic directional distributions.

[6] The primary purposes of this paper are, first, to determine whether or not α_4 appears to have a "universal" value, based on data covering a wide range of generation scales; second, to identify the most appropriate scaling velocity u for use with equations (2) and (3); and, third, to investigate whether or not our results are consistent with theoretical arguments based on the kinetic equation for weak interactions. To accomplish these goals, we use a compilation of data from six diverse sources: two from deep-ocean locations, two from nearshore sites and two from smaller enclosed basins. By incorporating data with different physical scales and wind speeds from different sites, our results will hopefully avoid empirically derived conclusions that are only appropriate over a small range of scales or at a single site. With u defined and α_4 estimated, nonlinear energy and momentum fluxes through the equilibrium range can be specified with no arbitrary constants, using complete integral forms for these properties. Combining such flux calculations with our empirical results should provide valuable insight into the applicability of weak interaction theory to the spectral equilibrium range.

2. Theoretical Perspective

[7] Many researchers [e.g., *Zakharov and Filonenko*, 1966; *Kitaigorodskii*, 1983; *Resio*, 1987; *Resio and Perrie*, 1991; *Young and van Vleddar*, 1993; *Resio et al.*, 2001] have shown that observations of the equilibrium range in nature, as well as in experimental basins, are consistent with the concept of a balance between wind input near the spectral peak region and fluxes of energy out of this region owing to nonlinear wave-wave interactions. For the purpose of this paper, a conceptual framework for partitioning a wind-wave spectrum into regions related to nonlinear fluxes of energy and basic energy balance concepts is given in Figure 1. Four spectral regions, based on the locations of three characteristic frequencies, f_0, f_{eq} and f_d, are shown here. A zero net flux of energy through a spectrum owing to nonlinear interactions occurs at f_0. A spectrum begins to take on an asymptotic, equilibrium range power law shape at f_{eq}. A dissipation range, where nonlinear energy fluxes are strongly absorbed by either wave breaking or viscosity, begins at f_d.

[8] In Figure 1, region I represents the spectral peak region. Its upper bound (at $f = f_0$) is defined as a frequency at which net energy flux is zero, so the net contribution to energy gain in region I owing to wave-wave interactions must also be zero (i.e., the positive front lobe and the portion of the negative lobe included up to $f = f_0$ are exactly equal). Thus net gain in total energy in this region must come only from wind input. Region II represents the transitional band between region I and the equilibrium range, region III. As in the equilibrium range, the net flux in region II is directed toward high frequencies (away from the spectral peak). Region IV is the part of the spectrum where all energy fluxes from regions II and III eventually must be lost to dissipative processes.

[9] It is assumed here that the three traditional deep-water source terms, wind input S_{in}, nonlinear wave-wave interactions S_{nl} and wave breaking S_{ds}, can occur in all regions of the spectrum to some degree. However, for a stable equilibrium to exist, the sum of these sources must equal zero. If the sum of wind and breaking wave source terms is not zero, S_{nl}, the divergence in the nonlinear energy fluxes, must be nonzero to maintain a net zero balance. Thus, over some range of frequencies,

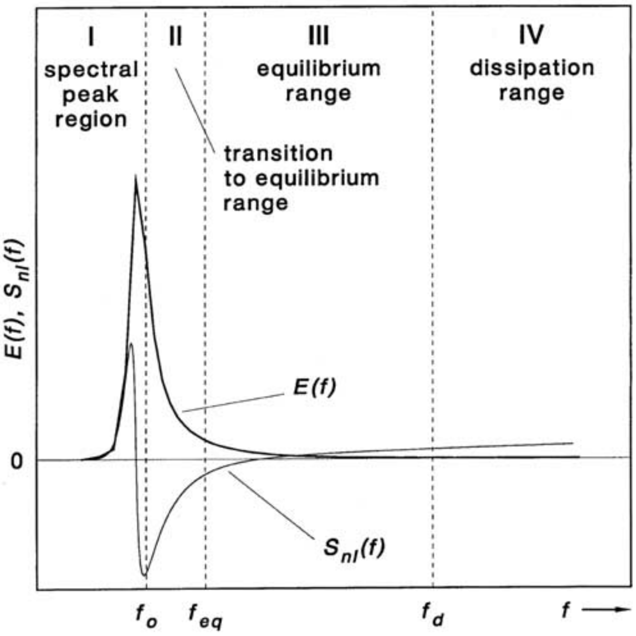

Figure 1. Conceptual depiction of a frequency spectrum $E(f)$, a characteristic shape of the wave-wave interaction source term $S_{nl}(f)$, and approximate locations of frequencies demarking four spectral regions that are identified by dominant energy flux processes.

$$S_{nl} \equiv \frac{\partial \Gamma_E}{\partial f} = S_{in} + S_{ds}, \tag{5}$$

where Γ_E is the net flux of energy through the spectrum. If S_{in} and S_{ds} exactly cancel each other in this range, the divergence would be identically zero and the flux would be exactly constant.

[10] Nonlinear interactions transfer energy from low to high frequencies and from high to low frequencies simultaneously. In some previous papers, the term flux has been used to describe positive directed fluxes (from low to high frequencies), while negative directed fluxes (from high to low frequencies) are termed inverse fluxes. Since Γ_E represents the net sum of fluxes in the two directions, it is given by

$$\Gamma_E = \Gamma_E^+ + \Gamma_E^-, \tag{6}$$

where superscripts "+" and "−" denote fluxes toward higher and lower frequencies, respectively. *Resio et al.* [2001] show both theoretically and numerically that nonlinear fluxes within the equilibrium range tend to force a spectrum toward an f^{-4} form (in deep water, toward a $k^{-5/2}$

form more generally). Data used in their study suggested that this characteristic equilibrium range form extended also to most situations with active wave generation. Thus their data showed that even in cases where significant wind inputs and wave breaking should be occurring, the $k^{-5/2}$ equilibrium form was maintained.

[11] *Resio et al.* [2001] show that, within the equilibrium range, the net flux of energy is from lower to higher frequencies (i.e., $\Gamma_E^+ > |\Gamma_E^-|$), and is given in a form equivalent to

$$\Gamma_E = C_{nl} g^{1/2} \beta^3, \tag{7}$$

where C_{nl} is a dimensionless coefficient that depends weakly on angular spreading and proximity to the spectral peak, and β is a wave steepness parameter equivalent to $\frac{1}{2}\alpha_4 u g^{-1/2}$ in equation (3). To a first approximation, the divergence of this flux can be written as

$$\frac{\partial \Gamma_E}{\partial f} \sim Z \frac{\partial \xi^3}{\partial f}, \tag{8}$$

where Z is a coefficient with suitable dimensions and ξ is a normalized spectral density of the general form

$$\xi = \frac{2F(k) g^{1/2} k^{5/2}}{\alpha_4 u} = \frac{F(k) k^{5/2}}{\beta}, \tag{9a}$$

from equation (3), and which takes the deep-water, f-dependent form

$$\xi = \frac{(2\pi)^3 E(f) f^4}{\alpha_4 u g} = \frac{(2\pi)^3 E(f) f^4}{2\beta g^{3/2}} \tag{9b}$$

from equation (2). It should be noted here that, from equations (2) and (3), $\xi \equiv 1$ if the f^{-4} (or $k^{-5/2}$) power law is followed exactly. The approximation (8) is reasonably accurate as long as dominant interactions involve waves that are all in the same vicinity within the spectrum. Integration of equations (5) and (8) from $f = f_{eq}$ (the low-frequency end of spectral region III in Figure 1, typically about two to three times the spectral peak frequency) to some arbitrary higher frequency leads to

$$\Gamma_E(f) - \Gamma_E(f_{eq}) \sim Z \int_{f_{eq}}^{f} \frac{\partial \xi^3}{\partial f} df \sim \int_{f_{eq}}^{f} [S_{in}(f) + S_{ds}(f)]\, df. \tag{10}$$

Two points are worth noting in equation (10). First, the divergence term has a cubic dependence on energy densities; thus a relatively small deviation in the slope from its equilibrium form can produce a large net flux divergence. Second, because the right-hand side is an integral, the local slope will depend on the rate of local input at a given frequency to the accumulated input from f_0 to that frequency.

[12] There has been considerable debate among researchers regarding the relative role of different source terms in the energy balance within wave spectra. *Kitaigorodskii* [1983] argued that spectral densities within the equilibrium range are primarily controlled by the condition of constant nonlinear energy flux. *Phillips* [1985] argued that it is possible to maintain an equilibrium range with a characteristic f^{-4} shape, even for situations in which the other source terms are significant, provided that the wind input and wave breaking terms both exhibit f^{-4} behavior. From equation (10), we see that any net gain or loss of energy within the equilibrium range would tend to force the spectrum away from an f^{-4} shape (i.e., the ξ of equation (9b) would not be constant), even if the external source balance (wind plus breaking) had an f^{-4} dependence; however, if the nonlinear term was very small compared to the other terms, this effect might be negligible. For a net gain (wind input exceeding wave breaking) and significant nonlinear interactions, the equilibrium spectrum would have to fall off less steeply than f^{-4} for the flux divergence to achieve a local energy balance. For a net loss at these frequencies (wave breaking exceeding wind input), the spectrum would fall off more steeply than f^{-4} for the flux divergence to balance the system. If the net effect of $S_{in} + S_{ds}$ is negligible within the equilibrium range, the flux of energy and ξ should be constant. In an alternative interpretation, ξ could be approximately constant through this range if the nonlinear fluxes are negligible compared to $S_{in} + S_{ds}$; hence it is important to examine estimated flux rates in an absolute sense, and not to speculate that just because they can produce an f^{-4} behavior in the equilibrium range, they are capable of effecting the observed behavior.

[13] As noted previously, there is a frequency f_0 near the spectral peak where the net nonlinear flux is zero, i.e.,

$$\Gamma_E(f_0) = \Gamma_E^+(f_0) + \Gamma_E^-(f_0) = 0, \tag{11}$$

so that, at lower frequencies (region I in Figure 1), the primary source of energy can only be wind input. Though the net nonlinear flux is zero at f_0, the separate positive and negative directed fluxes are not necessarily zero. In fact, computations show that the separate fluxes typically are very large at f_0. Consequently, the behavior of these fluxes plus the effects of any additional sources at frequencies between f_0 and f_{eq} (region II of Figure 1) are very important for characterizing the energy flowing out of region II and into region III (i.e., across f_{eq}).

[14] On the basis of an expression given by *Resio and Perrie* [1991], the positive directed energy flux past frequency f_a, with corresponding wave number modulus k_a following equation (4), has the form

$$\Gamma_E^+(f_a) = \iiint\!\!\oint C^2 D \left|\frac{\partial W}{\partial \boldsymbol{n}}\right|^{-1} ds\, H\left(-\oint C^2 D \left|\frac{\partial W}{\partial \boldsymbol{n}}\right|^{-1} \boldsymbol{ds}\right) \cdot H(|\boldsymbol{k}_3| - k_a) H(k_a - |\boldsymbol{k}_1|) d\boldsymbol{k}_3 d\boldsymbol{k}_1, \tag{12}$$

where C^2 is the coupling coefficient for the interacting waves, $\boldsymbol{n}$ and $\boldsymbol{s}$ are transformed wave number coordinates, D is a sum of triplets of energy densities for resonant interactions within the spectrum, $H(x)$ is the Heaviside function ($H(x) = 1$ for $x \geq 0$, $H(x) = 0$ for $x < 0$) and $W = f_1 + f_2 - f_3 - f_4$, where subscripts denote the different waves involved in each interaction. The contour integration in equation (12) is around loci such that $W = 0$. An expression

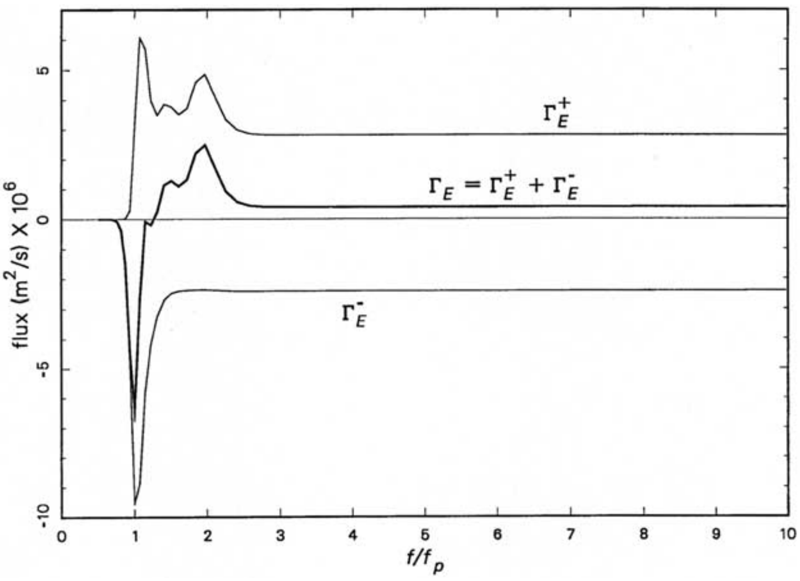

Figure 2. Computed positive directed $\Gamma_E^+(f)$ and negative directed $\Gamma_E^-(f)$ nonlinear energy fluxes and their sum $\Gamma_E(f)$ plotted versus f/f_p for the spectrum defined by equation (13). Here, $\Gamma_E = 0$ at $f/f_p \equiv f_0/f_p \approx$ 1.2, which identifies the no net flux lower bound of region II (transition region) in Figure 1. All fluxes become approximately constant for a broad range of frequencies beginning at $f/f_p \equiv f_{eq}/f_p \approx 2.5$, which identifies the lower bound of region III (equilibrium range) in Figure 1. Within this equilibrium range the net flux Γ_E is positively directed so that in the absence of significant wind input or wave breaking the only source of energy is the net flux leaving region II at its high-frequency boundary $f = f_{eq}$.

for $\Gamma_E^-(f_a)$ is identical to equation (12) except we reverse the negative sign preceding the contour integral in the left-most Heaviside argument. These expressions are evaluated following methods given by *Resio and Perrie* [1991] and *Resio et al.* [2001]. Readers are referred to those sources for computational details.

[15] Figure 2 gives the results of computed fluxes $\Gamma_E^+(f), \Gamma_E^-(f)$ and their sum $\Gamma_E(f)$ for the class of f^{-4} spectra defined by

$$E(f,\theta) = \alpha_4 ugf^{-4}\Psi\left(\frac{f}{f_p}\right)\Phi(\theta-\theta_0), \tag{13a}$$

where f_p is the spectral peak frequency, the peak shape function $\Psi(f/f_p)$ is

$$\Psi\left(\frac{f}{f_p}\right) = \begin{cases} \gamma^{e^{(f/f_p-1)/2\sigma^2}} & f/f_p \geq 1 \\ (f/f_p)^4\gamma^{e^{(f/f_p-1)/2\sigma^2}} & f/f_p < 1 \end{cases} \tag{13b}$$

and the angular spreading function $\Phi(\theta - \theta_0)$ of wave direction θ about mean wave direction θ_0 satisfies

$$\int_0^{2\pi} \Phi(\theta-\theta_0)d\theta = 1. \tag{13c}$$

For this case, $\alpha_4 = 0.01$, $u = 10$ m/s, $f_p = 0.1$ Hz, $\gamma = 3$, $\sigma = 0.08$, $\theta_0 = 0$ and $\Phi(\theta) = \frac{4}{3\pi}\cos^4\theta$. In this figure, we see that f_0 is located at about $1.2f_p$. This is typical of results for this class of spectra with $\gamma = 3$ and a $\cos^4$ angular spreading function. In fact, because the flux equals the integral of S_{nl}, the location of f_0 is constrained to be at the point where $\int_0^{f_0} S_{nl}(f)df = 0$. In other words, the positive area in the low-frequency lobe of S_{nl} must just balance the portion of the central negative lobe of S_{nl} to the left of f_0. Hence the location of f_0 (for single-peaked spectra, and given that such a value exists) is essentially always within the negative lobe of S_{nl} located near the spectral peak. For very peaked spectra, this location tends to be closer to the spectral peak than for spectra with low peakedness.

[16] As seen in Figure 2, the positive and negative directed fluxes both become approximately constant over an extended range of frequencies beginning at about $2.5f_p$. This frequency defines the approximate lower bound f_{eq} of the equilibrium range, which extends to the end of the integration range. Through this range, the positive directed flux is larger than the negative directed flux, supporting our interpretation of Figure 1, with a dominant nonlinear flow of energy from lower to higher frequencies in both regions II and III. The positive net flux $\Gamma_E(f_{eq})$ at f_{eq} is the total amount of energy exiting region II and should equal the integrated net gain of energy owing to wind input minus wave breaking throughout region II.

[17] Figure 3 shows plots of average ξ (based on equation (9a)) and their standard deviations in discrete bands of f/f_p for all observations in each of the six data sets described later in this paper. In the plot for Currituck Sound, examples are given of curves to which the data would conform if obeying k^{-3} (equivalent to f^{-5} in deep water) and k^{-2} (f^{-3} in deep water) power law shapes, assuming $f_{eq}/f_p = 1.5$. These alternate forms clearly do not fit the data very well. Even though some random deviations and some possibly periodic variations in ξ are seen,

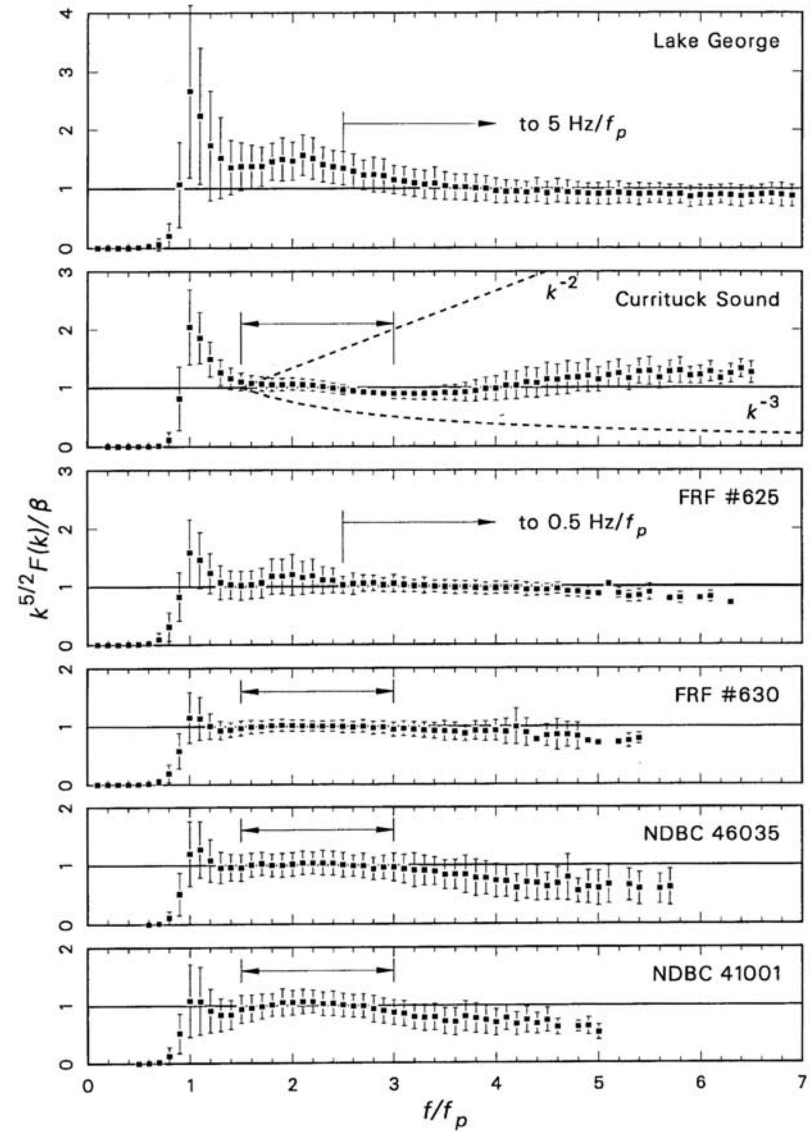

Figure 3. Means (squares) and standard deviations (error bars) of normalized wave number spectra within discrete bins of f/f_p. Horizontal arrows indicate ranges of f over which β were fitted. Shifted and extended ranges for Lake George and FRF 625 data reduce biasing effects on β estimates owing to evident spectral harmonics near $f = 2f_p$. Dashed lines indicate how data would appear if obeying alternative k^{-2} or k^{-3} power law models within an equilibrium range originating at $f_{eq} = 1.5f_p$.

the general tendency is for ξ to remain approximately constant through a finite range of frequency in each of the data sets. It should be noted that, because energy flux depends on the cube of spectral density, it would not require a very strong deviation from $k^{-5/2}$ behavior to accommodate a moderate net input or loss of energy due to wind input or wave breaking. Thus Figure 3 does not necessarily support or contradict arguments that the net gain or loss of energy in the equilibrium range is exactly zero. However, at least within the theoretical context presented here, these data indicate that net energy gains or losses are not so strong that they require large flux divergences to compensate for them.

[18] We can examine aspects of the energy balance within a spectrum by considering processes in region II of the spectrum within the framework developed above. Since the net nonlinear flux is zero at region II's lower boundary, wind input must exceed wave dissipation in region II in order to supply a positive directed flux past the low-frequency boundary of region III and into the equilibrium range. The net gain of energy in region II (wind input minus wave dissipation) must be balanced by the net nonlinear flux through its high-frequency boundary. Assuming that dissipative processes in wave generation can be scaled in a form functionally consistent with wind input, then, under steady, uniform conditions, equation (5) becomes

$$S'_{in}(f) - S_{nl}(f) = S'_{in}(f) - \frac{\partial \Gamma_E(f)}{\partial f} = 0. \qquad (14)$$

where the prime on S'_{in} denotes that the wind input has been replaced by an effective, or net, wind input. Integrating equation (14) over the width of region II from f_0 to f_{eq} with the conditions that $\Gamma_E(f_0) = 0$, $\Gamma_E(f_{eq}) = C_{nl}g^{1/2}\beta^3$ from equation (7) and $\beta = \frac{1}{2}\alpha_4 u g^{-1/2}$ leads to

$$\int_{f_0}^{f_{eq}} S'_{in}(f)df = \frac{1}{8}\alpha_4^3 C_{nl}u^3 g^{-1} \sim u^3 g^{-1}. \qquad (15)$$

[19] In equation (15) the precise interpretation of u is somewhat indeterminate in at least two senses. First, is u simply a surrogate for wind speed, or does it involve other, perhaps wave-related, parameters? Second, if u is wind-related, what wind speed parameter is most suitable for this application? In this paper, we shall investigate three potential wind speed parameters for application to this equation. These are u_{10}, the wind speed at a fixed reference level of 10 m above the mean water surface, u_*, the friction velocity $(=(\tau/\rho_a)^{1/2}$, where τ is wind stress and ρ_a is air density), and u_λ, the wind speed at an elevation that is a fraction λ of the spectral peak wavelength as proposed by *Donelan and Pierson* [1983], *Resio et al.* [1999], and others.

[20] On the basis of considerations of work rates in a boundary layer, one might assume that net energy transfer rates input waves are proportional to the cube of any one of these wind speed parameters. Alternatively, *Resio and Perrie* [1989] provide arguments that the net wind source term integrated from f_p to a frequency that is within the equilibrium range might vary as $u_*^2 c_p/g$ if a constant proportion of wind momentum is transferred to the wave field. Thus an alternative model for the equilibrium range velocity can be taken as $u \sim (u_*^2 c_p)^{1/3}$. For completeness, we shall also examine the alternative models $u \sim (u_{10}^2 c_p)^{1/3}$ and $u \sim (u_\lambda^2 c_p)^{1/3}$.

[21] Since it is possible that there also exists a small threshold wind scale u_0 below which a model given by equation (2) or (3) is no longer valid, a more general form for u can be written as

$$u = u_a - u_0, \qquad (16)$$

with

$$u_a = \begin{cases} u_* \\ u_{10} \\ u_\lambda \\ \left(u_*^2 c_p\right)^{1/3}, \\ \left(u_{10}^2 c_p\right)^{1/3} \\ \left(u_\lambda^2 c_p\right)^{1/3} \end{cases} \qquad (17)$$

as our final six candidates for a dynamic velocity scale. In this paper, we shall rely on observations to help discriminate among these various forms (and to set u_0 as necessary), and then investigate the consistency of these findings with weakly nonlinear theory.

3. Data

[22] Sources of data selected for analysis here include two deep-ocean buoys maintained by the National Data Buoy Center (NDBC, www.ndbc.noaa.gov), two nearshore sensors maintained by the U.S. Army Engineer Research and Development Center's Field Research Facility (FRF, www.frf.usace.army.mil), a site on the east side of Lake George, Australia [*Babanin et al.*, 2001], and a site in Currituck Sound, which abuts the landward side of the barrier island upon which the FRF resides. Figures 4–6 show the locations of the sites used in this study. Figure 4 shows the approximate location of one of the NDBC buoy sites, 46035, in the Bering Sea. The other NDBC buoy site, 41001, is in the Atlantic Ocean, about 300 km east of Cape Hatteras. Its approximate location is shown in Figure 5 (top), which also shows the general location of the FRF. Figure 5 (middle) shows the general area of the FRF, and includes locations of FRF gauge 630, a nondirectional Waverider buoy about 6 km offshore, FRF gauge 625, a Baylor gauge affixed to the seaward end of the FRF pier about 500 m offshore, and the instrumented sled about 900 m from the eastern shore of Currituck Sound. Figure 6 shows the location of the Lake George experiment site. Anemometers were located directly above wave sensors at all sites except for FRF 625 and 630, where winds were measured at the landward end of the FRF pier (Figure 5 (bottom)), and subsequently adjusted to be more representative of winds at the gauge sites. Appendix A describes this adjustment as well as additional information about the data sets and basic analysis methods used here. Table 1 describes primary instrumentation and ranges of environmental parameters included in data from these sites.

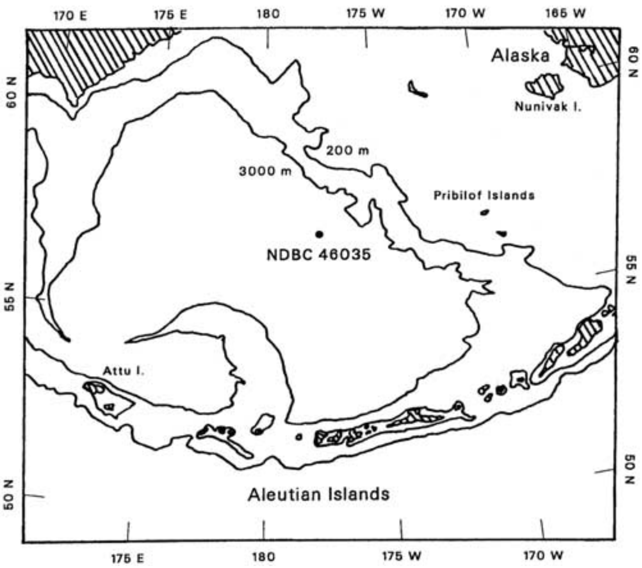

Figure 4. Approximate location of NDBC wind and wave buoy site 46035 in the Bering Sea.

[23] In choosing these sites, we sought to obtain observations from a very broad range of conditions where the present model formulation is valid. Four dimensionless parameters are relevant in this regard and are based on k_{eq}, the wave number at the low-frequency end of the equilibrium range (here taken to correspond with $f_{eq} = 1.5f_p$), water depth h, variance-based characteristic wave height H_{mo}, spectral peak wave number k_p, spectral peak phase speed c_p and wind speed scale u_a. The four dimensionless parameters are: equilibrium range relative depth

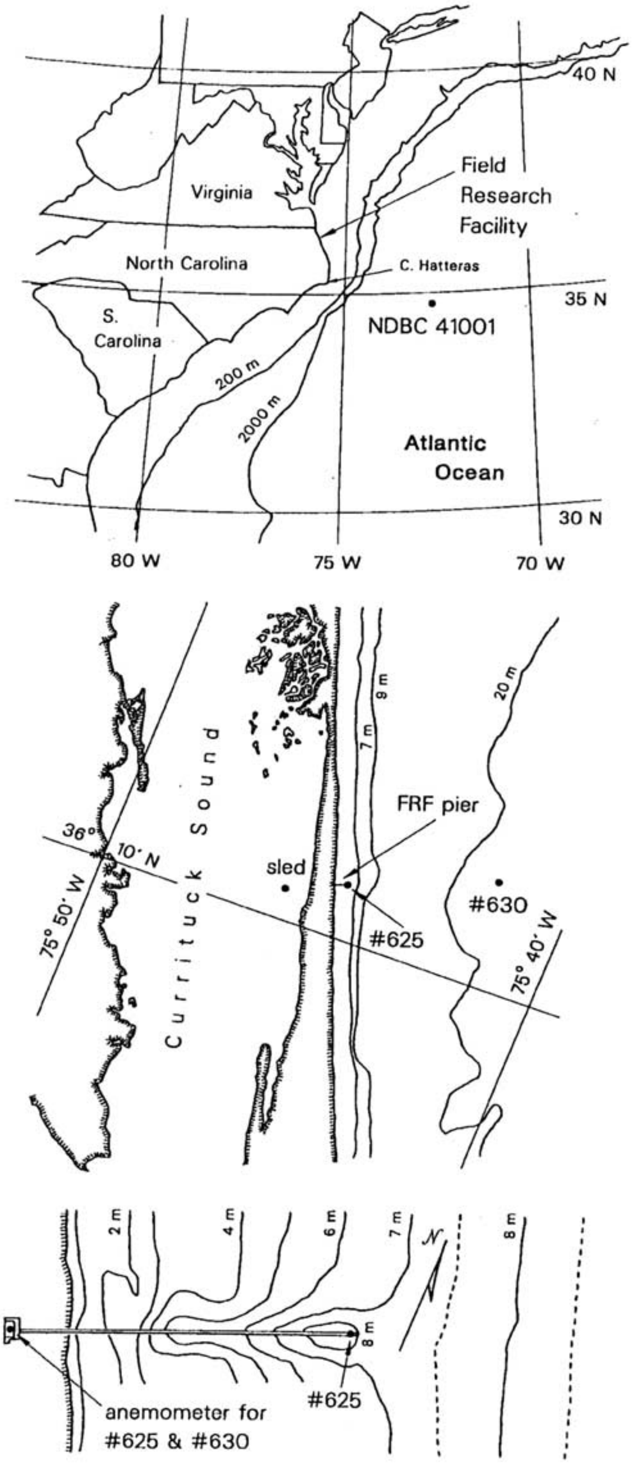

Figure 5. Locations of four data sites: (top) approximate locations of NDBC buoy site 41001 and the FRF; (middle) an enlarged view near the FRF showing the locations of FRF 630 (Waverider buoy), FRF 625 (Baylor gauge), and the instrumented sled in Currituck Sound; and (bottom) the 600-m FRF pier, the position of FRF 625 and the anemometer used to estimate winds for FRF 625 and FRF 630. Anemometers were horizontally collocated with wave gauges at the other two sites.

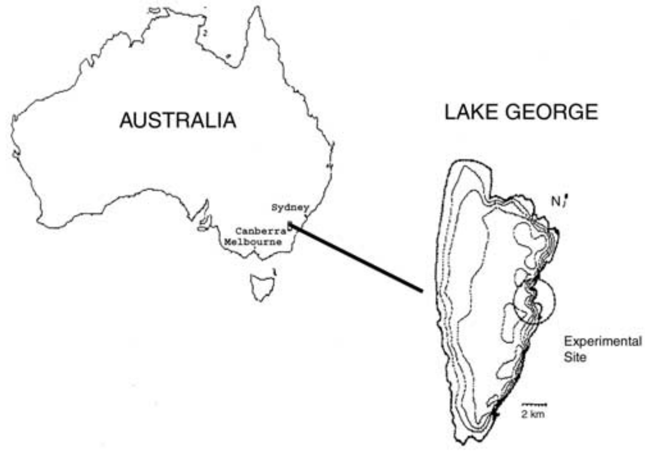

Figure 6. Site map for Lake George data. Anemometer and wave gauges were horizontally collocated about 50 m from the eastern shore. Depth contours are drawn at 0.5 m intervals, with the deepest contours at 2 m [*Babanin et al.*, 2001].

$k_{eq}h$, relative wave height H_{mo}/h, an indicator of validity of weak interaction theory $\frac{1}{2}H_{mo}k_p/\left(k_ph\right)^3$ and inverse wave age u_a/c_p (often characterized as u_{10}/c_p).

[24] For the first of these, there is an approximate theoretical lower limit $k_{eq}h \approx 0.7$ below which the wave number dependence of the equilibrium range may change form owing to depth-related variations in the behavior of the coupling coefficient in equation (12) [*Resio*, 1987]. *Zakharov* [1999] has shown that for $k_{eq}h < 0.3$, the spectrum should asymptotically tend toward a $k^{-4/3}$ form. Here, we use $k_{eq}h$ instead of his parameter kh to reflect the fact that his theoretical argument is strictly valid only within the equilibrium range and not in the spectral peak region. In data used here, the smallest $k_{eq}h = 0.76$, and so extends nearly to the lower limit of validity of the present model. The largest $k_{eq}h$ exceeds 1000, so the range of relative depth in these data is quite large.

[25] Relative wave height is important in two ways. On the one hand, H_{mo}/h is an indicator of shallow-water wave breaking. If this parameter becomes greater than about 0.5, depth-induced wave breaking may become a significant source term in the spectral energy balance, and the simple concept of an energy balance between wind input and nonlinear fluxes utilized here may not be valid. For the present data, $0.0004 < H_{mo}/h < 0.4$, so we do not expect too great an influence on our results owing to breaking waves. On the other hand, H_{mo}/h is an indirect indicator of the validity of the weak interaction theory employed here. *Zakharov* [1999] has shown that, for the statistical theory of weak interactions to be formally valid, the "Stokes number," defined as $N = ka/(kh)^3$, where, in this context, a is wave amplitude, has some stringent limitations. Specifically, these are $N \ll 1$ for directionally narrow-banded spectra and $(kh)^2N = a/h \ll 1$ for directionally broad spectra. If we take $a \approx \frac{1}{2}H_{mo}$ for Zakharov's arguments, then $a/h \approx \frac{1}{2}H_{mo}/h < 0.2$ for the present data, and his second condition is approximately met. An approximate Stokes number is $N \approx \frac{1}{2}H_{mo}k_p/\left(k_ph\right)^3$, and, for the present data, $6 \times 10^{-10} < N < 1.03$. Only about 9% of the cases have $N > 0.2$, so most of the data are approximately valid, even if they have narrow directional distribu-

Table 1. Site Names, Instrumentation, and Parameter Ranges for Data Used in Analysis[a]

Site	Range of Observation Dates	Wave Sensor	h Range, m	H_{mo} Range, m	Wind Sensor	z_m, m	u_{10}, Range m/s
Lake George	Sept. 1997 to March 1998	capacitance gauge ∼1 mm diameter[b]	0.60–1.15	0.05–0.44	Aanderaa model 2740 speed 3590 direction	10	5.1–19.8
Currituck Sound	Oct. 2001 to April 2002	capacitance rod ∼4.6 mm diameter[c]	2.28–2.93	0.09–0.59	R.M. Young model 09101	5	5.0–15.7
FRF 625	Oct.1986 to April 1991	Baylor model 23766 impedance gauge	7.5–10.1	0.67–3.80	Weathermeasure Skyvane model 2101	19.4	5.1–24.4
FRF 630	Oct. 1986 to April 1991	Datawell nondirectional Waverider 0.7-m hull	18.8–21.6	0.91–4.72	Weathermeasure Skyvane model 2101	19.4	5.1–27.6
NDBC 46035	Oct., Nov., & Dec. of 1999 & 2000	12-m discus buoy	>3600	2.30–11.3	R. M. Young model 05103	10	7.5–23.9
NDBC 41001	Oct., Nov., & Dec. of 1999 & 2000	6-m NOMAD buoy	>4300	1.70–8.50	R. M. Young model 05103	5	9.7–24.4

[a]Here h is water depth, H_{mo} is variance-based wave height, z_m is nominal anemometer elevation above water surface, and u_{10} is estimated 10-m wind speed (see text) for all sites except Lake George and NDBC 46035, where it was measured directly. The z_m is treated as constant for all sites except Currituck Sound, where it was adjusted for variations in h. All anemometers were collocated with wave sensors except FRF 625 and 630, where data from the land-based sensor were adjusted to be more like over-water winds.
[b]Richard Brancker Research, LTD, Ottawa, Canada.
[c]Ocean Sensor Systems, Inc., Coral Springs, Florida, USA.

tions. If the spectra have broad directional distributions, then all of the data should be legitimate samples of weak interaction processes.

[26] Inverse wave age is commonly used as a measure of the stage of wave development during generation by the wind. Values near unity indicate full development, higher values suggest young, growing seas, and lower values suggest reduced wind forcing. For the present data, $0.4 < u_{10}/c_p < 6.6$, indicating that these observations extend from the swell domain through full development to include some very young seas. This range encompasses most conditions of practical consequence in nature, but does not extend into conditions typical of laboratory-scale wind flumes.

[27] More observations were available from our six data sources than were actually used. To ensure that samples were consistent with the simple model proposed here (single-mode spectra subject to active, following winds), data were objectively screened prior to analysis using three criteria. First, for sites located near land (Lake George, Currituck Sound, FRF 625 and FRF 630), only cases where winds had an onshore component were included. This condition helped establish that waves were subject to a well-established marine or lacustrine boundary layer with a reasonably well-modeled surface roughness. It also helped preclude cases with very young seas that would not be well resolved by most of the gauges used. The second criterion was that minimal swell coexisted with the wind sea. Where a spectrum was bimodal at its low-frequency end, it was required that the spectral density of the lower-frequency peak be less than 10% of the density at the other peak, or else the sample was excluded. The third criterion was that acceptable cases have $u_{10} > 5$ m/s. Like the first criterion, this helped ensure that wave signals could be reasonably resolved by all the extant instrumentation and, furthermore, that surface roughness estimates of the *Charnock* [1955] form used here (see Appendix A) dominated alternative roughness scales that may be important in flows with low Reynolds numbers.

4. Results

[28] As already seen in Figure 3, observed spectra, when compensated by $k^{-5/2}$, exhibit near-zero slopes over the range of frequencies consistent with our concept of an equilibrium range. Less consistent with these observations are alternative power law models, which follow k^{-3} (or f^{-5} in deep water) or k^{-2}(f^{-3} in deep water). As suggested by Figure 3, an equilibrium range extends at least to $4f_p$, and, possibly, beyond. There are what appear to be shoaling wave harmonics near $f/f_p = 2$ in Lake George and FRF 625 data, but slopes are quite flat outside this region. Deviant behavior is seen in Currituck Sound data at high frequencies, owing probably to a high data discretization noise floor that induces a slight upward bias in low-energy parts of these spectra. There is a noticeable tendency for normalized spectra from the two NDBC buoys to become downward sloping for $f/f_p > 3.5$. Such a pattern might be taken as supporting the existence of a spectral region controlled by wave breaking as suggested by *Forristall* [1981] and postulated by *Hansen et al.* [1990]. However, it could also be an artifact of the measurement systems at these sites, since both of these are large buoys that are less responsive to higher frequency waves. Because the focus of this paper is on spectral energies in the equilibrium range, we will leave this discrepancy as a topic for future research.

[29] Following the form of equation (9a), β was estimated from each observation as the average of $F(k)k^{5/2}$ over a

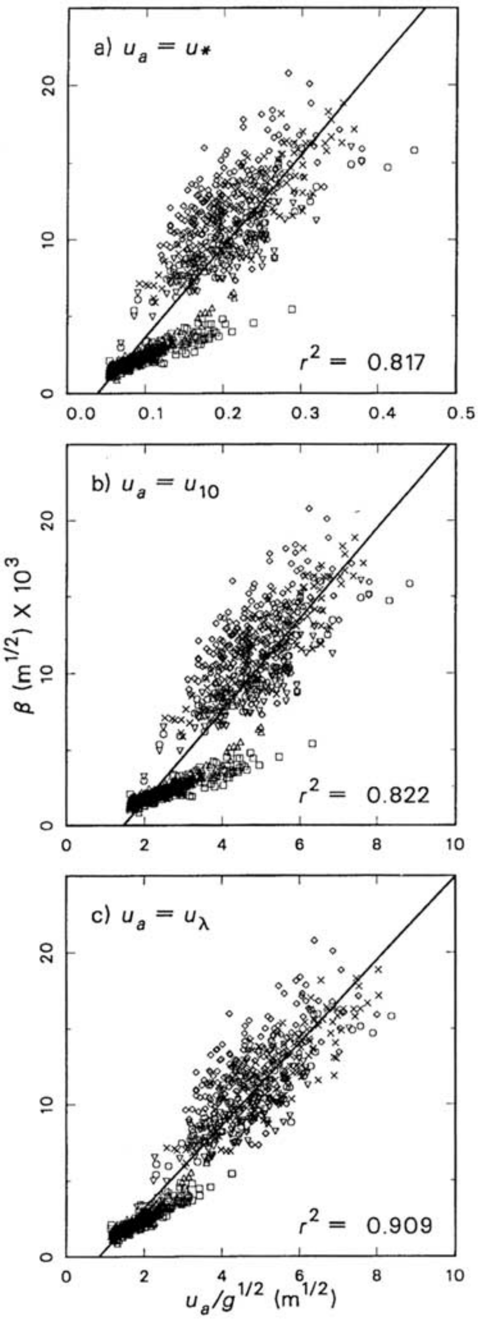

Figure 7. Correlation (coefficient r^2 indicated) of β with $u_a/g^{1/2}$ for (a) $u_a = u_*$, (b) $u_a = u_{10}$, and (c) $u_a = u_\lambda$ using data from Currituck Sound (open triangles, point up), Lake George (open squares), FRF 630 (open circles), FRF 625 (open triangles, point down), NDBC 41001 (open diamonds), and NDBC 46035 (crosses).

region of the spectrum taken as representative of the equilibrium range (see Appendix A). In this section, we relate the set of estimated β from all of our data to each of our six candidate velocities u_a. As β has the dimension square root length, we correlate it with the parameter $u_a g^{-1/2}$ to be consistent both dimensionally and with the form of equation (3). Note that such an analysis contains little or no spurious partial correlation because β is estimated purely from spectral densities away from the spectral peak, and u_a depends primarily on wind speed. Though three of the velocity scales investigated do contain $c_p^{1/3}$, the small exponent indicates that the scales depend only weakly on f_p and this should introduce very little statistical contamination owing to partial correlation.

[30] Figures 7a–7c and 8a–8c show results for the six different candidate velocity scales investigated here. Table 2 contains the regression and correlation coefficients

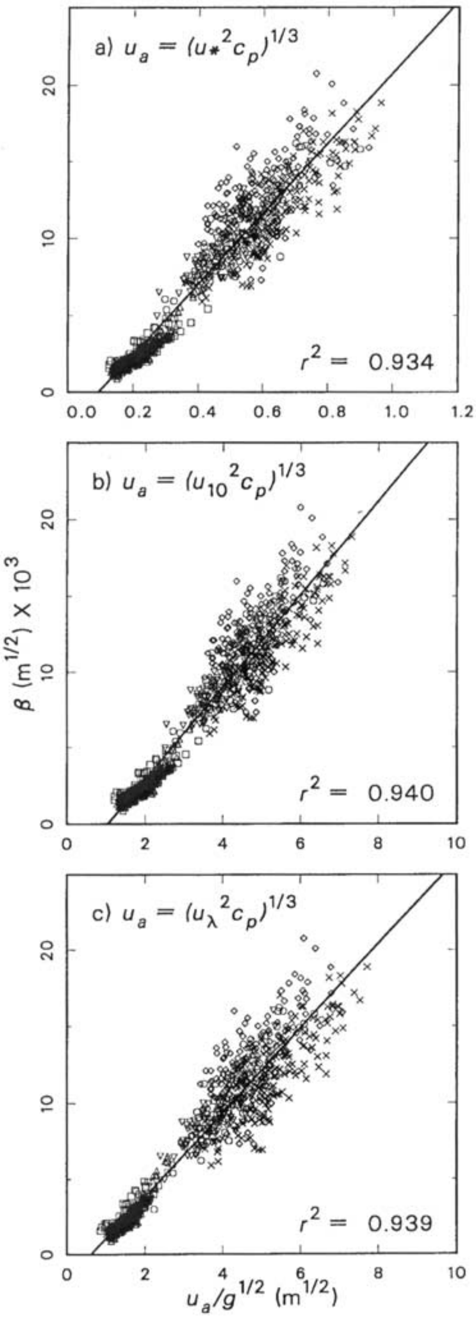

Figure 8. Correlation (coefficient r^2 indicated) of β with $u_a/g^{1/2}$ for (a) $u_a = (u_*^2 c_p)^{1/3}$, (b) $u_a = (u_{10}^2 c_p)^{1/3}$, and (c) $u_a = (u_\lambda^2 c_p)^{1/3}$ using data from Currituck Sound (open triangles, point up), Lake George (open squares), FRF 630 (open circles), FRF 625 (open triangles, point down), NDBC 41001 (open diamonds), and NDBC 46035 (crosses).

Table 2. Parameters of the Model $\beta = \frac{1}{2}\alpha_4(u_a - u_0)g^{-1/2}$ Deduced From Linear Regressions (Correlation Coefficient r^2) Shown in Figures 7 and 8 for Each of Six Candidate Velocity Scales

u_a	α_4	u_0, m/s	r^2
u_*	0.119	0.122	0.817
u_{10}	0.00596	4.56	0.822
u_λ	0.00545	2.62	0.909
$(u_*^2 c_p)^{1/3}$	0.0459	0.291	0.934
$(u_{10}^2 c_p)^{1/3}$	0.00609	3.25	0.940
$(u_\lambda^2 c_p)^{1/3}$	0.00553	1.92	0.939

corresponding to these plots. In Figures 7a–7c, which involve the simple velocity scales $u_a = u_*$, u_{10} and u_λ, respectively, it is seen that a linear dependence of β appears to fit data from individual sites relatively well, but data from different sites exhibit very different slopes when analyzed in this manner. In particular, slopes for data from the two small-basin sites (Lake George and Currituck Sound) differ markedly from those evident for the large-basin sites. In Figures 8a–8c, involving $u_a = (u_*^2 c_p)^{1/3}$, $(u_{10}^2 c_p)^{1/3}$ and $(u_\lambda^2 c_p)^{1/3}$, respectively, a single regression line appears to fit the data from all sites more uniformly, and the slope deviations evident in Figure 7 are much reduced. Partly because of this, correlation coefficients in Figure 8 are uniformly higher than those in Figure 7.

[31] For all of the velocity scales used in Figures 7 and 8, there is a positive offset of the intersection of the regression curve and the x axis. This offset implies that there is, for these data, a finite value of u_0 in the general form of u given by equation (16). For regressions of the form $\beta = au_a g^{-1/2} + b$ and the result $F(k) = \beta k^{-5/2} = \frac{1}{2}\alpha_4(u_a - u_0)g^{-1/2}k^{-5/2}$ from using equation (16) in equation (3), it is easy to see that $\alpha_4 = 2a$ and $u_0 = -bg^{1/2}/a$. These derived parameters are given in Table 2 for each of the linear regression curves in Figures 7 and 8.

[32] Figures 9a–9c present plots of observed β normalized by their regression estimates $au_a g^{-1/2} + b$ as functions of $k_{eq}h$ for data from Lake George, Currituck Sound, FRF 625 and FRF 630 only. The reason for using a reduced data set here is to focus on sites where relative depth is approaching shallow water, rather than extending the x axis to the large $k_{eq}h$ typical of the deep-water sites. For completeness, the mean values of the data for which $k_{eq}h$ exceeds the cutoff value for these plots is shown on the far right-hand side of each figure, along with the RMS range of the data. As can be seen here the deep-water values are consistent with the shallow-water values. Figures 9a–9c are based on regressions using velocity scales $u_a = (u_*^2 c_p)^{1/3}$, $(u_{10}^2 c_p)^{1/3}$ and $(u_\lambda^2 c_p)^{1/3}$, respectively. Two aspects of these plots can be noted. First, the variation of normalized β with relative depth is small for all three of these wind scales and essentially zero for wind scaling based on $(u_\lambda^2 c_p)^{1/3}$. Second, $(u_\lambda^2 c_p)^{1/3}$ scaling seems to provide a more consistent representation for the normalized β in the reduced data set, particularly in the range $6 \le k_{eq}h \le 10$, where scaling forms based on $(u_*^2 c_p)^{1/3}$ and $(u_{10}^2 c_p)^{1/3}$ both appear to diverge significantly from their mean values in the range $k_{eq}h < 6$.

5. Discussion

[33] Results obtained in section 4 suggest that velocity-scaling forms for β that include a phase-speed dependence

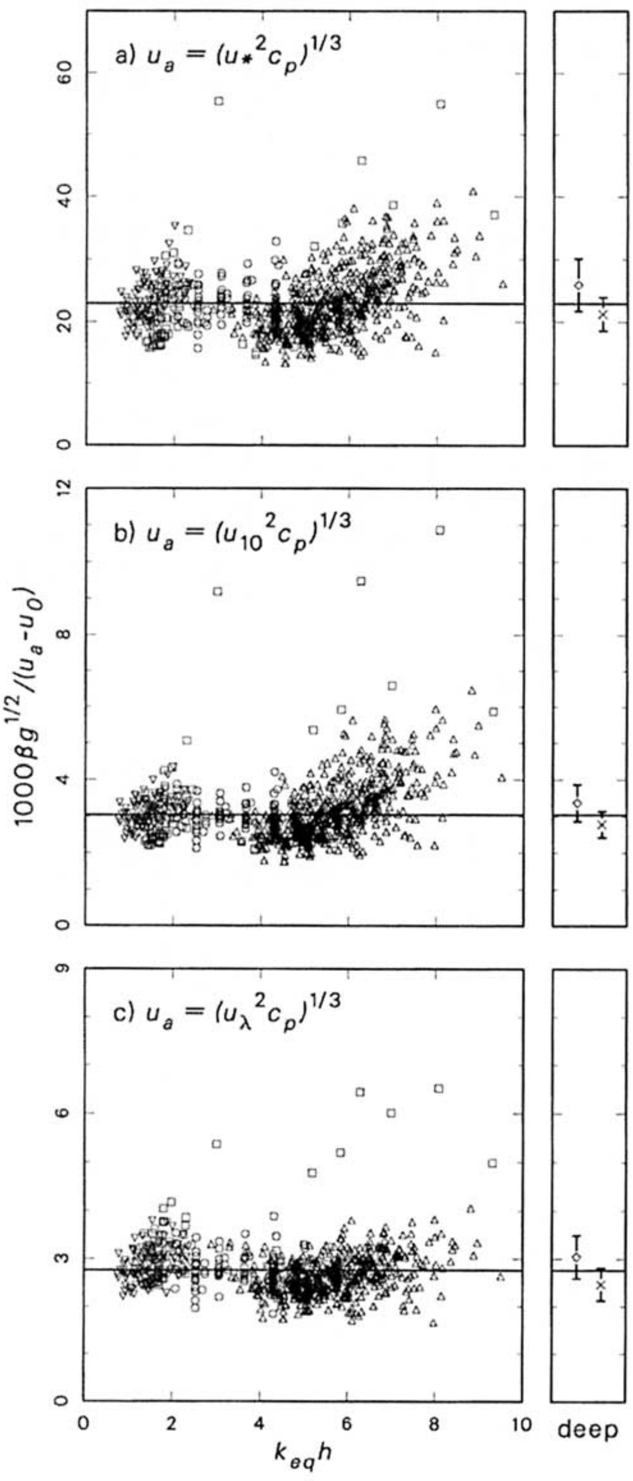

Figure 9. Estimates of $\frac{1}{2}\alpha_4 = \beta g^{1/2}/(u_a - u_0)$ as functions of equilibrium range relative depth $k_{eq}h$, with k_{eq} corresponding to a nominal equilibrium range frequency $f_{eq} = 1.5f_p$ and u_0 the regression offset velocity from Table 2 for (a) $u_a = (u_*^2 c_p)^{1/3}$, (b) $u_a = (u_{10}{}^2 c_p)^{1/3}$, and (c) $u_a = (u_\lambda^2 c_p)^{1/3}$ using data from Currituck Sound (open triangles, point up), Lake George (open squares), FRF 630 (open circles), and FRF 625 (open triangles, point down). Solid horizontal lines are based on regression estimates of α_4 from Table 2.

provide a better fit to the data than those based on a linear wind speed parameter alone. Furthermore, such forms avoid site-dependent slope variations implicit in parameterizations based on wind speed alone. As is particularly evident in Figure 9, the most effective wind-scale parameter, at least in terms of reducing scatter around what is presumed to be a "universal" constant, is wind speed taken at a fraction of the spectral peak wavelength above the water surface. On the basis of results by *Resio et al.* [1999], the fraction is taken here as 0.065. This value is not too far removed from the height coefficient derived by *Miles* [1993] for the "critical layer" for wind input, which in his theory is 0.045 times wavelength. Separate computations with data presented here indicate that results are fairly insensitive to choices of height coefficients between these two values.

[34] Another interesting aspect of our results is the apparent lack of dependence of β on relative depth. As shown in Figure 9, no significant variation in the $\beta - u$ relationship is exhibited in any of our finite depth data sets. It is difficult to reconcile this lack of dependence of β on $k_{eq}h$ with the existence of dominant depth-limited wave breaking or bottom friction effects within the equilibrium range in these depths. Recently, *Herbers et al.* [2002] showed that spectral peak energy losses in waves at the FRF site appear to be consistent with the calculated cascade of energy into the high-frequency spectral tail (where it is presumably lost because of wave breaking) in their Boussinesq model. The cascade of energy described by Herbers et al. is dimensionally consistent with nonlinear energy fluxes presented here, since the phase-dependent interactions in that model are derivable from the phase-dependent Zakharov equation. *Resio* [1987] and *Resio et al.* [2001] have also provided arguments suggesting that the scaled wave-wave interactions, rather than bottom friction, may be the dominant energy-loss mechanism at the FRF site.

[35] This paper has added confirmation that a $k^{-5/2}$ equilibrium range occurs in nature over a wide range of conditions. We have determined the value for α_4 in equation (3) in terms of each of the six candidate wind-scaling parameters used here. On the basis of the evidence presented in this paper, the "best" representation of the equilibrium range is given by

$$F(k) = \frac{1}{2}\alpha_4\left[\left(u_\lambda^2 c_p\right)^{1/3} - u_0\right]g^{-1/2}k^{-5/2} \tag{18}$$

with constants α_4 = 0.00553 and u_0 = 1.92 m/s. This appears to hold true for a wide range of wave generation scales, at least for $k_{eq}h > 0.7$. Although this shows that the shape of the equilibrium range is consistent with weak interaction theory, it does not show whether or not the absolute magnitudes of the fluxes are consistent with the theory. The remainder of our discussion will focus on addressing this issue in terms of the energy/momentum entering the wave spectrum in regions I and II.

[36] It has been long been thought that the majority of the wind energy/momentum enters the spectrum at frequencies considerably higher than f_{eq} [*Stewart*, 1974; *Snyder et al.*, 1981; *Kudryavtsev and Makin*, 2002]. Momentum input into waves is generally assumed to be of the form $\tau(f) \sim (u/c)^p E(f)(2\pi f/c)$, where $\tau(f)$ is the momentum flux into the spectrum at frequency f and p is typically taken to be in the range of 1 to 2 [*Snyder et al.*, 1981; *Resio and Perrie*, 1989; *Kudryavtsev and Makin*, 2002]. Input of this functional form in conjunction with f^{-4} based spectral shapes, as described by *Resio and Perrie* [1989] can be evaluated numerically from the integral

$$M_R \sim u^2 \int_{f_1}^{f_2} \frac{E(f)\omega}{c^{p+1}} \Psi\left(\frac{f}{f_p}\right) df$$

where M_r is the total amount of momentum entering a spectral region between frequencies f_1 and f_2. For spectral peakedness values in the range of 1 to 4, numerical solutions for the ratio of momentum entering regions I + II to the momentum entering regions III + IV indicate that 70% or more of the total momentum transfer occurs at frequencies higher than f_{eq}. On the basis of consistency with field evidence and detailed numerical studies, *Kudryavtsev and Makin* [2002] argue that no more than about 50% of the total momentum leaving the atmosphere enters the wave field directly. On the basis of their analyses and consistency with the momentum input given above, no more than 15% of the total momentum flux from the atmosphere to the water would be directly entering the wave field in regions I and II defined here. On the other hand, recent arguments have been advanced that a larger proportion of the energy/momentum may be entering the spectrum near the spectral peak [*Alves and Banner*, 2003] and that a substantial portion of this momentum is lost to local dissipative processes in this part of the spectrum. In either case (little dissipation in regions I and II or substantial dissipation in regions I and II), the net nonlinear energy fluxes within the equilibrium range are still positive (i.e., directed toward higher frequencies) at f_{eq}; thus a positive net source (wind input minus dissipation) into region II must exist to balance the flux out of region II into the equilibrium range.

[37] It is clear that alternative arguments for the absolute proportion of momentum entering the spectrum in region II can be hypothesized, depending on the magnitude of wave dissipation assumed. In fact, as long as dissipation is hypothesized to scale consistently with wind input, one could adjust the absolute magnitudes of the wind input and wave dissipation by an arbitrary constant, under the constraint that it must be smaller than the total momentum transfer from the atmosphere. In subsequent discussions given below, it is recognized that we are dealing with net input (wind input minus local wave dissipation) and not wind input alone.

[38] From equation (7) and the results shown here, we can represent the "variance" fluxes through the equilibrium range as

$$\Gamma_E = \frac{1}{8} C_{nl}\alpha_4^3 (u_a - u_0)^3 g^{-1}, \tag{19}$$

where u_a is one of the six candidate wind speed scales, and α_4 and u_0 are the corresponding regression constants from Table 2. Since C_{nl} can be determined directly from the interaction integral, equation (19) contains no free parameters and can be used to provide an independent estimate for total wind input in spectral region II, under the assumption that wave breaking is negligible. The consistency or lack of consistency of this estimate with existing wave generation and air-sea interaction concepts gives at least a first-order check on the validity of the theoretical framework described in this paper.

[39] The variance flux of equation (19) can be converted to energy flux by multiplying both sides of equation (19) by $\rho_w g$, where ρ_w is water density. This yields a dimensionally correct expression of nonlinear energy flux through the equilibrium range. If the result $\rho_w g \Gamma_E$ is divided by a phase speed c_{II} characteristic of spectral region II, we obtain a measure of the momentum flux from the atmosphere that enters spectral region II and causes the net wave energy flux from region II into the equilibrium range. The total momentum flux from the air is $\rho_a u_*^2$; hence the ratio $R = (\rho_w g \Gamma_E)/(\rho_a u_*^2 c_{II})$ represents the fraction of net atmospheric momentum input entering region II that contributes to the net flux through the equilibrium range.

[40] To estimate R, we use results based on the parameter $u_a = (u_*^2 c_p)^{1/3}$ because the interpretation of this parameter in terms of momentum fluxes from the atmosphere is more direct than that based on $u_a = (u_\lambda^2 c_p)^{1/3}$, and it is still reasonably representative of observations, as seen in Figure 8a. Using equation (19) in the definition of R and simplifying the result, we find

$$R = \frac{1}{8} C_{nl} \alpha_4^3 \left(1 - \frac{u_0}{u_a}\right)^3 \frac{c_p}{c_{II}} \frac{\rho_w}{\rho_a}. \tag{20}$$

From computations involving realistic spectra in section 2, a typical value of $C_{nl} \approx 0.4$, and its range is relatively small. We take $\alpha_4 = 0.0459$ from Table 2, let c_{II} correspond to $f_{eq} \approx 2f_p$ so that $c_p/c_{II} \approx 2$, and note that $\rho_w/\rho_a = O(10^3)$. The bracketed term in equation (20) has two asymptotes, one where $u_a \rightarrow u_0$ and one where $u_a \gg u_0$. On the first asymptote, R goes to zero, suggesting that the atmospheric input may result in no net flux through the equilibrium range for some threshold wind speed. Our data contain values for the bracketed term as low as about 0.2. On the other asymptote, the bracketed term in equation (20) approaches unity; however, the maximum ratio for u_a/u_0 in our data is only about 8.5. Thus the largest value for the bracketed term in our data is only about 0.7. Using these estimates, the value of R obtained from the nonlinear momentum fluxes into the equilibrium range is approximately 1.5% to 4.5%.

[41] These values for R (the retained momentum fraction within region II) appear consistent with estimates of retained total momentum within the wave field from *Hasselmann et al.* [1973] and *Resio and Perrie* [1989], which suggest that in deep water the wave field retains about 5% of the total momentum leaving the atmosphere. This fraction should be approximately equal to the net portion of momentum entering the wave spectrum in region I. Thus it is not unreasonable that about 1.5% to 4.5% might be entering the spectrum in region II. If dissipation is small in regions I and II, these results would imply that about 6-8% of the total momentum leaving the atmosphere would be concentrated into regions I and II. If dissipation is not small, the actual percentages of momentum inputs into these regions could be somewhat higher. Additional theoretical, laboratory, and field evidence will be required to obtain a firm estimate of the absolute momentum transfer rate into regions I and II (i.e., the total momentum input into these regions before dissipation is subtracted); however, results here appear to be consistent with our estimates of the magnitude of nonlinear fluxes entering the equilibrium range.

[42] The variation in the bracketed term in equation (20) indicates that energy levels within the equilibrium range, under a constant wind speed, will increase with fetch. At noted earlier, the values of both f_0 and f_{eq} vary systematically with peakedness, which has also been found to vary systematically with dimensionless fetch [*Donelan et al.*, 1985], so it is possible that this variation is related statistically to this observed phenomenon.

6. Conclusions

[43] An analysis of data sets from two deep-water ocean sites, two nearshore ocean sites and two small-fetch, enclosed basins has shown the following: (1) wind waves subject to a large range of wind speeds, fetches and peak spectral periods have equilibrium ranges well represented by a $k^{-5/2}$ spectral form, at least for cases used here where $k_{eq}h > 0.7$; (2) energy levels within the equilibrium range can be represented by a universal relationship involving wind speed and the phase speed of the spectral peak, even for sites in relatively shallow water; (3) velocity parameterizations, which include the phase speed of the spectral peak along with wind speed, appear to provide significantly improved estimates of equilibrium range energy levels than those which include wind speed alone; (4) wind estimates based on a reference level located at a constant fraction of the spectral peak wavelength above the mean water level appear to give a slightly more consistent representation of energy levels in the equilibrium range than either wind estimates from a fixed 10-m level or friction velocity; (5) flux rates from solutions to the full integral solution for weak interactions are consistent with estimated magnitudes of atmospheric momentum fluxes that must be conveyed from the near-peak portion of the spectrum into the equilibrium range.

Appendix A

A1. Currituck Sound Observations

[44] References at the beginning of section 3 provide gauging and site descriptions for all data sources except Currituck Sound. At this site (Figure 5 (middle)), an instrumented sled was deployed from October 2001 to April 2002 to complement the small-scale wave data obtained from Lake George. The sled was fitted with an array of nine, surface piercing, capacitance wave gauges and an anemometer (5 m nominal elevation). Collections consisted of 42-min records of winds and water levels digitally sampled every 0.2048 s. Representative spectra used here consist of averaged synoptic spectra from the nine individual gauges. The discretization noise floor influenced spectral estimates at frequencies above 2 Hz, especially in very low energy conditions. Thus acceptable data were constrained to have $H_{mo} > 0.09$ m and $f_p < 0.7$ Hz. This constraint provided reliable estimates of β within the nominal equilibrium range used here. We note that high-frequency mean spectral estimates that rise above the $k^{-5/2}$ normalization in Figure 3 are likely due to the noise floor bias.

[45] A precision bathymetric survey by the FRF staff, spanning 500 m north-south and 3000 m east-west in the vicinity of the sled position, indicated a nearly flat bottom, with variations of about 0.4 m/km in typically 2.5-m depths, everywhere except for a steep submerged bank about 500 m east of the sled location. A NOAA chart of Currituck Sound was found to be in gross agreement with these observations, and indicated a generally flat bottom for several km to the west of the sled position. Irregular FRF survey lines and local lore indicated shoal areas near the sled position to the north and south. To ensure results from relatively unobstructed fetches, sled data were retained only for winds from within a 140° arc extending from 60° north of west to 80° south of west (see Figure 5). The sound bottom varies from hard sand to soft mud, is irregularly patchy, and often layered. At the sled site, the bottom was hard sand, but the bottom character along any upwind transect is probably a mix of textures.

A2. Case Sampling and Spectral Analysis

[46] We acquired sample observations from sites with near-continuous monitoring (FRF and NDBC) by isolating 20 to 30 storm events and winnowing individual cases through the screening process described in section 3. For Lake George and Currituck Sound, we screened all available data. Conventional Fourier analysis was used to estimate frequency spectra $E(f)$, with degrees of freedom (dof) varying from site to site. Spectra from Lake George have 58 dof; from Currituck Sound, 120 dof; from FRF 625 and FRF 630, 192 dof; and from NDBC 41001 and NDBC 46035, 24 dof. The relatively low dof of the NDBC spectra may account for some of the scatter in results from these sites evident in Figures 7 and 8. We defined wave number spectra from frequency spectra using the variance density-preserving form $F(k) = E(f)\partial f/\partial k$, with $\partial f/\partial k$ evaluated using equation (4).

A3. Adjustment of FRF Wind Speeds

[47] It is well known that land-based wind measurements can be significantly different from winds measured over water. At the time of acquisition of data from FRF 625 and FRF 630 used here, the nearest anemometer was located at the landward end of the FRF pier (Figure 5 (bottom)). We compared 4,296 wind measurements from this anemometer with synoptic measurements from a second anemometer at the same elevation on a tower at the seaward end of the FRF pier during a subsequent period when both anemometers were deployed. A mean ratio of wind speeds computed in discrete 10°-wide direction bins indicated little difference between the two sites for winds blowing directly onshore, but, for highly oblique winds, land-based wind speeds were lower than pier end winds by as much as 35%. Wind directions were relatively unaffected. Consequently, we multiplied land-based wind speeds by the mean ratio of pier end wind speed to land-based wind speed corresponding with land-based wind direction. This objective adjustment yields an improved estimate of winds local to FRF 625 and FRF 630.

A4. Estimation of Wind Parameters

[48] We deduced wind parameters from measured wind speed u_m at elevation z_m assuming a conventional logarithmic wind profile with neutral stratification. A *Charnock* [1955] expression provided an estimate of surface roughness as $z_0 = \alpha_c u_*^2/g$, with $\alpha_c = 0.015$ following *Resio et al.* [1999]. Iterative solution of the wind profile equation $u_m = (u_*/\kappa)\ln(z_m g/\alpha_c u_*^2)$, where $\kappa(= 0.41)$ is von Karman's constant, gives an estimate of friction velocity u_*. Wind speed at constant height $z_{10} = 10$ m is then $u_{10} = (u_*/\kappa)\ln(z_{10}g/\alpha_c u_*^2)$. Reference elevation at a fraction λ of spectral peak wavelength L_p is $z_\lambda = \lambda L_p = 2\pi_\lambda/k_p$, where k_p is spectral peak wave number and $\lambda = 0.065$ as used by *Resio et al.* [1999]. Wind speed at this elevation is then $u_\lambda = (u_*/\kappa)\ln(z_\lambda g/\alpha_c u_*^2)$.

A5. Estimation of β

[49] At a wave number k_n for which discrete spectral density is $F(k_n)$, a local estimate β_n of the coefficient for data following a $k^{-5/2}$ power law is $\beta_n = k_n^{5/2}F(k_n)$. The average of such local estimates over a range of indices corresponding to frequencies that nominally bound the equilibrium range provided our estimates of $\beta = \frac{1}{n_2-n_1+1}\sum_{n=n_1}^{n_2} k_n^{5/2}F(k_n)$. For all sites except Lake George and FRF 625, we chose indices n_1 and n_2 such that corresponding frequencies were in the range $1.5f_p \le f_n \le 3f_p$, following *Donelan et al.* [1985]. For Lake George and FRF 625, there appeared (see Figure 3) to be harmonic peaks at frequencies near $2f_p$, probably owing to shoaling transformations at these sites of waves near f_p. These peaks thus have apparent energy levels above what would exist in spectra not subject to shoaling, and estimates of β using data in the frequency range used at the other sites would be biased high. To avoid this bias, we modified the fitting range to include all frequencies satisfying $f_n \ge 2.5f_p$. Though this modified range extended to high frequencies, notably to 5 Hz in Lake George data, we note that we saw no extended region that deviated significantly from $k^{-5/2}$ behavior, and that the mean normalized spectra for Lake George and FRF 625 in Figure 3 are quite well behaved. The modification is significant; had we used the same fitting range for these two sites as for the other four sites, β would be, on average, 9% higher for FRF 625 data and 28% higher for Lake George data than what we have found with the modified fitting range.

[50] **Acknowledgments.** The research presented in this paper was conducted under the U.S. Army Corps of Engineers RDT&E program. The Chief of Engineers has granted permission for publication. Many thanks to Ian Young and Alex Babanin for providing the Lake George data used in this study. The Currituck Sound expedition would not have been possible without the intrepid and frequently brilliant contributions of Brian Scarborough and Kent Hathaway, and the stalwart efforts of Bill Grogg, Dan Freer, Ray Townsend, and Mike Leffler. The ongoing efforts of the National Data Buoy Center are much appreciated.

References

Alves, J. H. G. M., and M. L. Banner (2003), Performance of a saturation-based dissipation-rate source term, I, Modeling the fetch-limited evolution of wind waves, *J. Phys. Oceanogr.*, *33*, 1274–1298.

Babanin, A. V., I. R. Young, and M. L. Banner (2001), Breaking probabilities for dominant surface waves on water of finite constant depth, *J. Geophys. Res.*, *106*, 11,659–11,676.

Charnock, H. (1955), Wind stress on a water surface, *Q. J. R. Meteorol. Soc.*, *81*, 639–640.

Donelan, M. A., and W. J. Pierson (1983), The sampling variability of estimates of spectra of wind-generated gravity waves, *J. Geophys. Res.*, *88*, 4381–4392.

Donelan, M. A., J. Hamilton, and W. H. Hui (1985), Directional spectra of wind-generated waves, *Philos. Trans. R. Soc. London, Ser. A*, *315*, 509–562.
Forristall, G. Z. (1981), Measurements of a saturated range in ocean wave spectra, *J. Geophys. Res.*, *86*, 8075–8084.
Hansen, C., K. B. Katsaros, S. A. Kitaigorodskii, and S. E. Larsen (1990), The dissipation range of wind-wave spectra observed on a lake, *J. Phys. Oceanogr.*, *20*, 1264–1277.
Hasselmann, K., et al. (1973), Measurements of wind-wave growth and swell decay during JONSWAP, *Ergänzungsheft Dtsch. Hydrogr. Z.*, *12*, 95 pp.
Herbers, T. H. C., N. R. Russnogle, and S. Elgar (2002), Spectral energy balance of breaking waves within the surf zone, *J. Phys. Oceanogr.*, *30*, 2723–2737.
Kitaigorodskii, S. A. (1962), Application of the theory of similarity to the analysis of wind-generated wave motions as a stochastic process, *Bull. Acad. Sci. USSR Geophys. Ser.*, *1*, 105–117.
Kitaigorodskii, S. A. (1983), On the theory of the equilibrium range in the spectrum of wind-generated gravity waves, *J. Phys. Oceanogr.*, *13*, 816–826.
Kudryavtsev, V. N., and V. K. Makin (2002), Coupled dynamics of short waves and the airflow over long surface waves, *J. Geophys. Res.*, *107*(C12), 3209, doi:10.1029/2001JC001251.
Miles, J. (1993), Surface-wave generation revisited, *J. Fluid Mech.*, *256*, 427–441.
Mitsuyasu, H. (1968), On the growth of wind-generated waves (I), *Rep. Res. Inst. Appl. Mech.*, *16*, 459–482.
Phillips, O. M. (1958), The equilibrium range in the spectrum of wind-generated waves, *J. Fluid Mech.*, *4*, 426–434.
Phillips, O. M. (1985), Spectral and statistical properties of the equilibrium range in wind-generated gravity waves, *J. Fluid Mech.*, *156*, 505–516.
Resio, D. T. (1987), Shallow water waves. I-Theory, *J. Waterw. Port Coastal Ocean Eng.*, *113*, 264–281.
Resio, D. T., and W. Perrie (1989), Implications of an f^{-4} equilibrium range for wind-generated waves, *J. Phys. Oceanogr.*, *19*, 193–204.
Resio, D. T., and W. Perrie (1991), A numerical study of nonlinear energy fluxes due to wave-wave interactions. part 1. Methodology and basic results, *J. Fluid Mech.*, *223*, 609–629.
Resio, D. T., V. R. Swail, R. E. Jensen, and V. J. Cardone (1999), Wind speed scaling in fully developed seas, *J. Phys. Oceanogr.*, *29*, 1801–1811.
Resio, D. T., J. H. Pihl, B. A. Tracy, and C. L. Vincent (2001), Nonlinear energy fluxes and the finite depth equilibrium range in wave spectra, *J. Geophys. Res.*, *106*, 6985–7000.
Snyder, R. L., F. W. Dobson, J. A. Elliott, and R. B. Long (1981), Array measurements of atmospheric pressure fluctuations above surface gravity waves, *J. Fluid Mech.*, *102*, 1–59.
Stewart, R. W. (1974), The air-sea momentum exchange, *Boundary Layer Meteorol*, *6*, 151–167.
Toba, Y. (1973), Local balance in the air-sea boundary processes on the spectrum of wind waves, *J. Oceanogr. Soc. Jpn.*, *29*, 209–220.
Young, I. R., and G. P. van Vleddar (1993), A review of the central role of nonlinear interactions in wind-wave evolution, *Philos. Trans. R. Soc. London, Ser. A*, *342*, 505–524.
Zakharov, V. E. (1999), Statistical theory of gravity and capillary waves on the surface of a finite-depth fluid, *Eur. J. Mech.*, *18*, 327–344.
Zakharov, V. E., and N. N. Filonenko (1966), The energy spectrum for stochastic oscillation of a fluid's surface, *Dokl. Akad. Nauk.*, *170*, 1992–1995.

C. E. Long and D. T. Resio, Coastal and Hydraulics Laboratory, U.S. Army Engineer Research and Development Center, Vicksburg, MS, USA. (donald.t.resio@erdc.usace.army.mil)

C. L. Vincent, Coastal Dynamics Program, Office of Naval Research, Arlington, VA, USA.